Preprints (www.preprints.org) | NOT PEER-REVIEWED | Posted: 24 October 2019 doi:10.20944/preprints201910.0273.v1

Peer-reviewed version available at Atmosphere 2019, 10, 750; doi:10.3390/atmos10120750

Article

Growth Rate of Gravity Wave Amplitudes Observed in Sodium Lidar Density Profiles and Nightglow Image Data

Fabio Vargas [1]*, Guotao Yang [2], Paulo Batista [3] and Delano Gobbi [3]

1 University of Illinois at Urbana-Champaign, USA; fvargas@illinois.edu
2 State Key Laboratory of Space Weather, Chinese Academy of Sciences, China; gtyang@spaceweather.ac.cn
3 National Institute for Space Research, Brazil; paulo.batista@inpe.br (P.B.); delano.gobbi@inpe.br (D.G.)
* Correspondence: fvargas@illinois.edu
† Current address: 306 N. Wright St., 5066 ECEB, MC-702, Urbana, Illinois, USA, 61801

Abstract: Amplitude growth rates of monochromatic gravity waves were estimated and compared from multiple instrument measurements carried out in Brazil. Wave dynamic parameters were obtained from sodium density profiles from lidar observations carried out in Sao Jose dos Campos (23°S, 46°W), while all-sky images of multiple airglow layers provided amplitudes and parameters of waves over Cachoeira Paulista (23°S, 45°W). Growth rates of gravity wave amplitudes from lidar and airglow imager data were consistent with dissipative wave behavior. Only a small amount of the observed wave events presented freely propagating behavior. Part of the observed waves presented saturated amplitude. The general saturated or damped behavior is consistent with diffusive filtering processes imposing limits to amplitude growth rates of the observed gravity waves.

Keywords: all-sky imager; sodium lidar; gravity waves; mesospheric nightglow; amplitude growth rate; wave dissipation

1. Introduction

Gravity waves play an important role in atmosphere dynamics due to their ability to transport momentum and energy from the lower to the upper atmosphere. Their influence on the mesospheric region (80-100 km) include heating through turbulence generated by breaking waves, transport and mixing of constituents, reversal of the zonal mean jets and mean flow acceleration through momentum flux transfer to the mean flow, modifying the dynamical conditions at those altitudes [1,2].

Freely propagating gravity waves (no dissipative waves) are expected to increase their amplitudes as $\sim \exp(\alpha z)$, where $\alpha = \frac{1}{2H}$ is the growth rate of freely propagating gravity waves, z is the altitude and H is the atmospheric scale height. The wave amplitude increases in order to conserve kinetic energy in response to the atmospheric density decreasing with the altitude [3]. Typical value of H is $\sim$6 km, and a wave generated at an altitude of 10 km is expected to have an amplitude $\sim$349 times larger at the mesospheric region ($\sim$90 km) than that measured at the generation altitude.

Frequently, instability processes (i.e. convective and/or dynamical), or diffusion (atmospheric viscosity) impose limits to the amplitude growth of gravity waves. Thus, departures from α (the amplitude growth of freely propagating waves) are observed, indicating that the wave is being dissipated. [4] have investigated high frequency gravity waves (<1 hour) disturbing the mesopause temperature by using wind/temperature lidar measurements. They have shown that gravity waves are basically saturated (no change in the wave amplitude over the observed altitude range) to over-damped below 100 km of altitude, while they are unsaturated to freely propagating above that level.

Preprints (www.preprints.org) | NOT PEER-REVIEWED | Posted: 24 October 2019 doi:10.20944/preprints201910.0273.v1

Peer-reviewed version available at Atmosphere 2019, 10, 750; doi:10.3390/atmos10120750

Also, [5] have shown that small period waves (<12 h) observed in rotational temperature of OH(6-2) and O_2(0-1) emissions tend to be strongly dissipated throughout the year. Gravity wave characterization has been also carried out using simultaneous measurements of the airglow intensity and temperatures by [6], and simultaneous measurements of the OH and O_2 emission layers were utilized to infer wave growth and dissipation. They have reported a high variability in the wave amplitude growth within a short altitude range of 7 km, i.e., the spatial separation between OH and O_2 layer centroids.

In this paper we use two different instruments (a Na lidar system and a nightglow all-sky imager) to estimate wave amplitudes and growth rates of gravity waves modulating the atmospheric fields at different altitudes in the mesopause region. The lidar and the imager sample different regions of the gravity wave spectra and provide complementary information about gravity wave modes present in Na density and airglow intensity data. The obtained results also give insights about the limiting processes taking place in the atmosphere in response to increasing wave amplitudes.

2. Instrumentation and Methodology

Gravity wave intrinsic parameters, amplitudes, and growth rates were obtained from lidar and all-sky imager data in this study. As both instruments provide wave amplitudes at different altitudes, amplitude growth rate of waves may be estimated by $\beta = \frac{\ln A_1/A_2}{\Delta z}$, where A_1 and A_2 are the amplitudes of a gravity wave at the altitude levels 1 and 2, respectively, and Δz is the distance between these levels. Here we refer to β as the growth rate of monochromatic waves in general, to distinguish from $\alpha = \frac{1}{2H}$, the growth rate of freely propagating waves (non dissipative waves), where H is the scale height.

A Na lidar system located in Sao Jose dos Campos (23°S, 46°W) provided sodium density vertical profiles from where 45 monochromatic vertically propagating gravity wavers were observed from 1994 to 2004. Na lidar measurements of these events have been reported by [7], while the gravity wave parameter estimation from the sodium profiles have been carried out by [8].

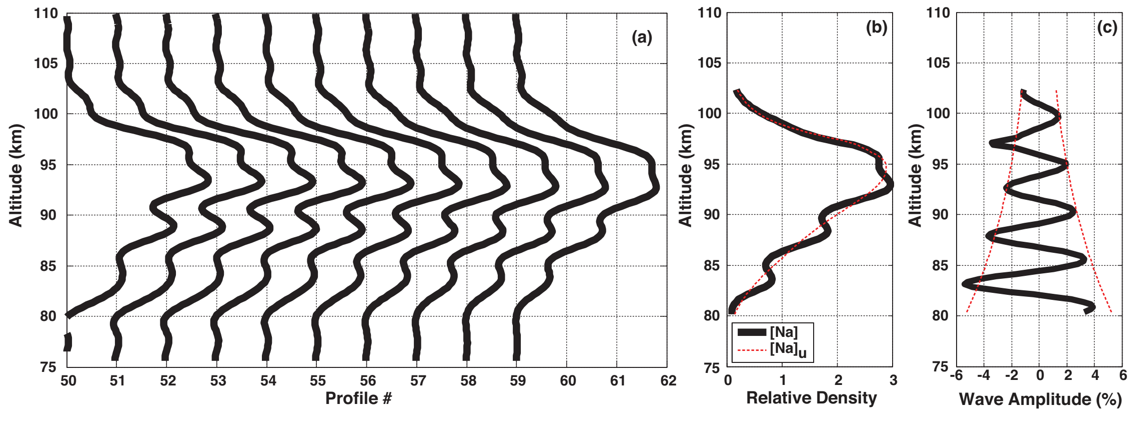

Figure 1. (a) Observed sequence of sodium density profiles taken on May 30, 1996 by a Na lidar system. (b) A single Na density profile superposed by an estimated background profile. (c) Wave amplitude obtained from (b). Notice the wave amplitude decreasing with altitude indicating that $\beta < 0$.

Fig. 1 shows how the monochromatic waves were identified in sodium lidar data. Fig. 1(a) shows a temporal series of vertical sodium profiles from 75-110 km, with temporal (spatial) resolution of 3 min (250 m). The sodium density profiles are first spatially and temporally low-pass filtered with cutoffs of about 1.5 km and 20 minutes, respectively. Coherent downward phase progression can be seen in Fig. 1. Additionally, Fig. 1(b) shows a single [Na] profile superposed to an estimated unperturbed $\overline{[Na]}$ profile. The relative wave amplitude perturbing the Na layer is given in Fig. 1(c), showing a decreasing wave amplitude as it propagates upward. For this specific case, the wave presents vertical wavelength

Preprints (www.preprints.org) | NOT PEER-REVIEWED | Posted: 24 October 2019 doi:10.20944/preprints201910.0273.v1

Peer-reviewed version available at *Atmosphere* **2019**, *10*, 750; doi:10.3390/atmos10120750

λ_z =4.6 km, amplitude of 2.46% relative to the ambient density (at 90km), and inverse growth rate $\frac{1}{\beta}$=-24 km. Wave periods, horizontal wavelengths, and phase velocities can be also estimated by using the technique described by [8].

On the other hand, a multicolor nightglow imager operating at Cachoeira Paulista (23°S, 45°W) provided images of the mesospheric nightglow layers for three emissions during 1999, 2000, 2004 and 2005. A description of this imaging system is given in [9].

In order to obtain dynamic parameters of observed gravity waves, we first preprocess the image dataset by performing usual corrections in every image (i. e., unwarping, star removal, coordinate transformation, detrending, and filtering). [10] present the preprocessing methodology used in this study. We focus in wave events occurring quasi-simultaneously in two or three nightglow layers. Fig. 2(a) shows an example of a strong gravity wave perturbing simultaneously the central area of images of three nightglow emissions. We have spatially filtered the image set in order to increase the contrast of wave crests by using the Butterworth filter with cutoff spatial frequencies at $\frac{1}{100}$ km^{-1} and $\frac{1}{10}$ km^{-1}. The result of filtering operation is presented in 2(b).

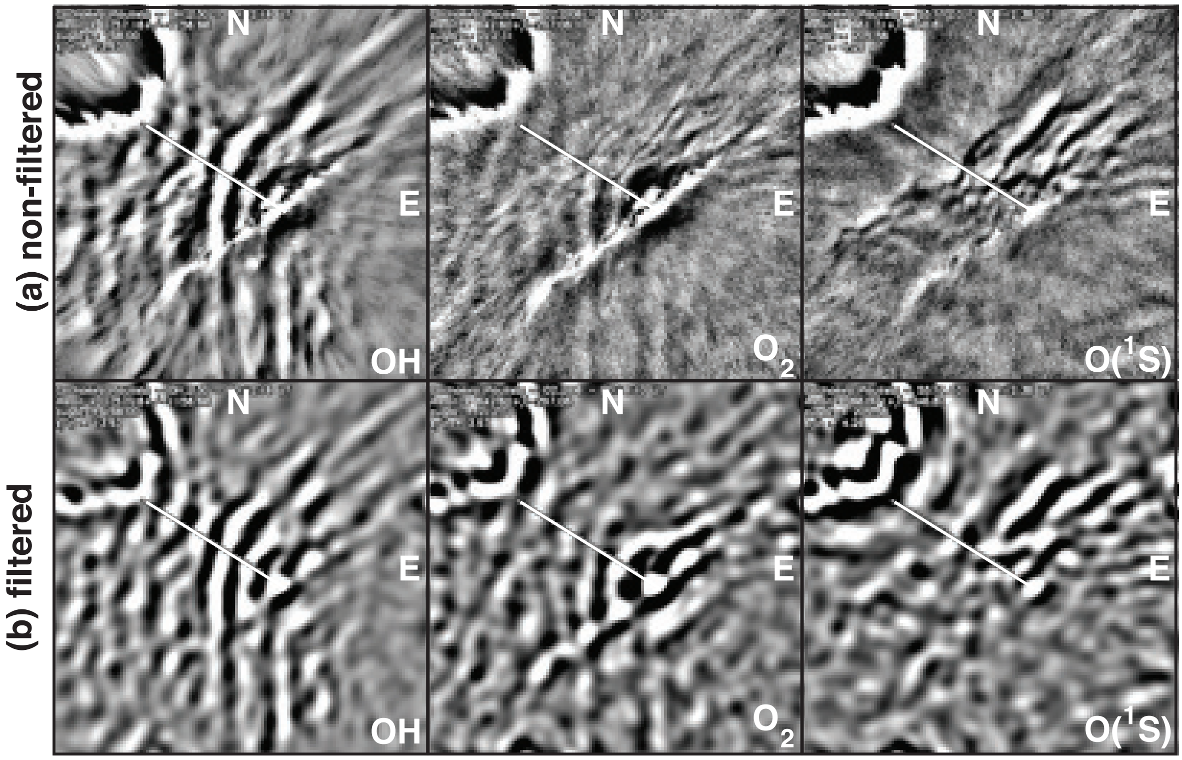

Figure 2. (a) a set of unwarped, non-filtered all-sky images of the OH, O_2 and O(^1S) airglow layers taken quasi-simultaneously on June 30, 2000 at Cachoeira Paulista, Brazil. A large amplitude gravity wave is perturbing all three layers. (b) The same set of images smoothed by a Butterworth spatial band pass filter with cutoff spatial frequencies at $\frac{1}{100}$ km^{-1} and $\frac{1}{10}$ km^{-1}. The straight lines indicate the pixels whose relative intensity values were extracted to estimate the wave amplitude for each layer.

Images of the OH, O_2 and O(^1S) emissions showing simultaneously prominent gravity wave events are then submitted to 1D cross-spectral analysis in order to deduce the wave horizontal wavelength, phase difference at different layer, relative amplitude and growth rate, propagation direction, phase velocity, and period. Due to differences in integration times of every emission and filter wheel sequence cycle in our imaging system, we have only been able to identigy 52 wave events disturbing simultaneously the layers in four years of observations.

The wave amplitude is obtained in one layer by extracting relative intensity $\frac{\Delta I}{I}$ along a straight line drawn perpendicularly to the wave fronts (see Fig. 2). Spatial series of pixel intensities along that straight line extracted from the images of each layer can be seen in Fig. 3(a). Pair of these series are

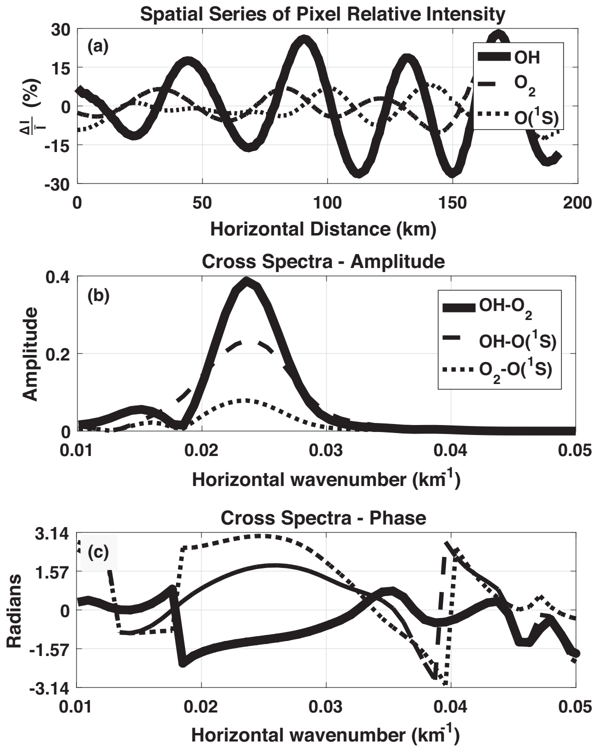

Figure 3. (a) spatial series of pixel of relative intensity extracted along the wave front disturbing the OH, O_2 and O(^1S) airglow layers in Fig. 2. (b) Amplitude and (c) phase cross-spectra calculated for each pairs of spatial series of the emissions. A prominent peak is evident around 0.025 km^{-1}, indicating a gravity wave of ∼40 km horizontal wavelength as the cause of the perturbations.

then subjected to cross-spectral analysis from where amplitude and phase periodograms are obtained. Fig. 3(b) and Fig. 3(c) show the amplitude and phase periodograms of the spatial series extracted from the images in Fig. 2.

The location of a spectral maximum in the amplitude periodogram indicates the horizontal wavelength of the perturbing wave. By integrating below that maximum value we obtain an estimation of the relative wave amplitude. Because the vertical distance Δz between the centroid of two given airglow layers is known, the amplitude growth rate is estimated by solving $\beta = \frac{\ln(A_2/A_1)}{\Delta z}$. As the wave perturbs all three layers at the same time, we observe a finite phase difference for every spatial series pair (Fig. 3(c)).

By applying the procedure above to the images in Fig. 2, we have obtained the following dynamical parameters for the observed gravity wave event: horizontal wavelength of ∼40 km, period of ∼30 minutes, propagation direction of 160°, apparent phase speed of ∼20 m/s, and amplitude of 15%, 7% and 5% in OH, O_2 and O(^1S) layers, respectively, indicating a dissipative wave.

3. Results

[8] identified 45 gravity events from analysis of ten years of sodium density profiles recorded by lidar, and we have identified 52 gravity events events from analysis of 4 years of airglow images. These two instruments sample distinct ranges of the gravity wave spectra.

Larger vertical scales accessed from lidar measurements are limited by the sodium layer thickness (∼15 km) and the shortest vertical wavelength is basically limited by the signal shot noise [11]. For this reason waves identified in lidar data by [8] presented vertical wavelengths ranging from 2.4 km to 9.3 km, with most of these waves (∼40%) ranging from ∼3 to ∼4 km. Observed wave periods ranged from 63 min to ∼20 hours, with maximal occurrence (66%) in the 100-300 min range. Gravity waves from lidar measurements presented long horizontal wavelengths ($32 < \lambda_h < 1887$ km), but with

Preprints (www.preprints.org) | NOT PEER-REVIEWED | Posted: 24 October 2019 doi:10.20944/preprints201910.0273.v1

Peer-reviewed version available at Atmosphere 2019, 10, 750; doi:10.3390/atmos10120750

a tendency of dominance of waves presenting λ_h <200 km. Wave amplitudes ranged from 0.77% to 8.4% of the ambient density, with an average value of 2.7%.

Gravity wave vertical wavelengths from imager measurements are larger than the airglow layer thicknesses [12]. Typical layer thickness varies from 8 to 10 km. Because of the observed airglow intensity is given by vertical integration of the volume emission rate of the emission, short vertical scale waves (λ_z <15 km) are difficult to observe once they self-interfere within the layer. The wave intensity perturbation is strongly attenuated for ground-based observations in that case. Imagers are able to observe short period waves (τ <1 hour) and fast phase speeds (c_o >40 m/s). The horizontal wavelength accessed with imager is limited by the field of view of the instrument. The lower limit is determined by the spatial resolution (ds) of each pixel , which is 1 km/pixel in this study. Spectral analysis of the events studied in here showed λ_h ranging from ~14 to ~78 km. The analysis of spatial series extracted from images revealed relative wave amplitudes ($\frac{\Delta I}{I}$) ranging from 0.6% to 15% for the OH, from 0.5% to 8.5% for O_2, and from 0.5% to 8.5% for $O(^1S)$ emissions, respectively.

Fig. 4 shows histograms for the amplitude growth rate (β) for waves observed in both imager and lidar data. Positive values of β (under-saturated region) indicate amplitude amplification, while negative values (over-damped region) indicate decreasing wave amplitudes. Values of β close to zero indicate that the amplitude does not change much as the wave propagates upward (saturated wave). Also, it is considered here that waves presenting β >7 are freely propagating waves, i.e., their amplitude increases as $\sim \exp(\alpha z)$.

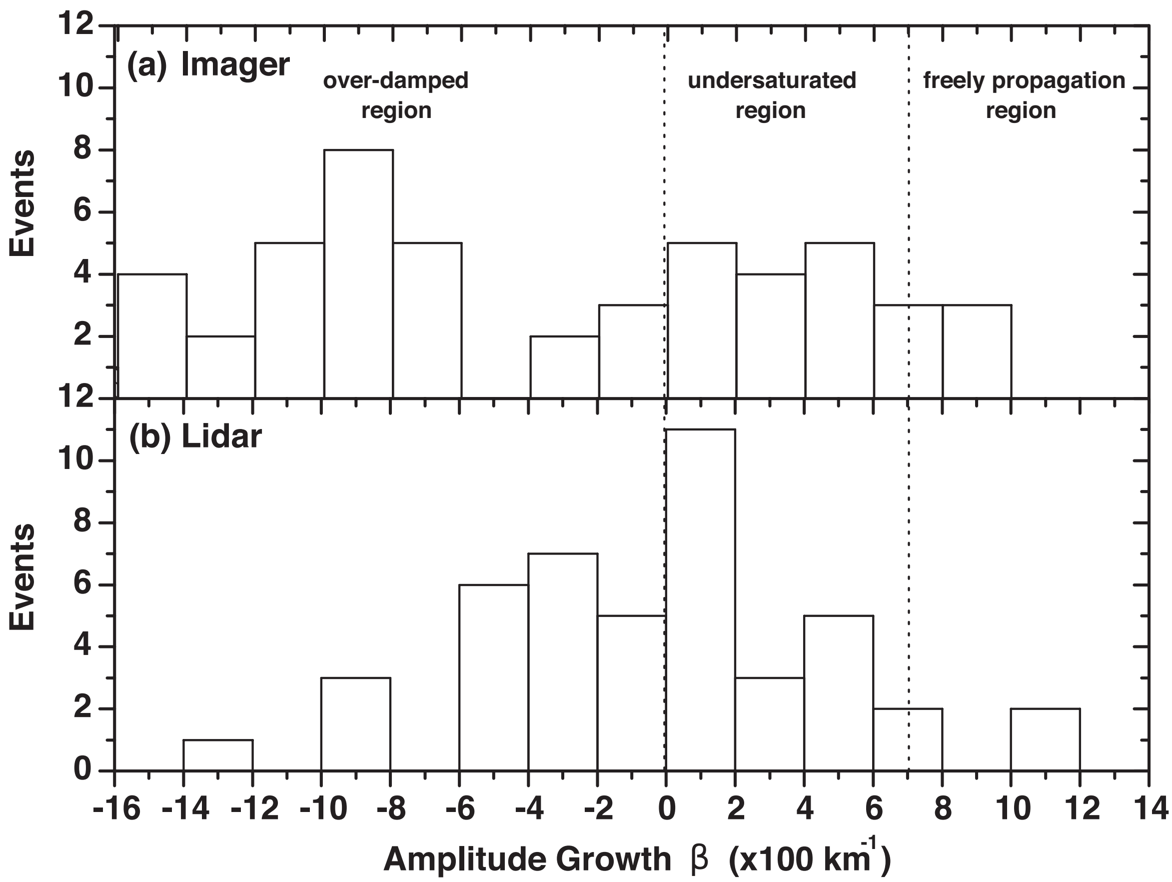

Figure 4. Amplitude growth of waves observed by (a) all-sky imager and (b) sodium lidar. Positive values of the growth rate indicate increasing gravity wave amplitudes. Negative values of β indicate amplitude attenuation as the wave propagates upward. Regions of distinct amplitude growth characteristics are indicated in the diagram.

Preprints (www.preprints.org) | NOT PEER-REVIEWED | Posted: 24 October 2019 doi:10.20944/preprints201910.0273.v1

Peer-reviewed version available at Atmosphere 2019, 10, 750; doi:10.3390/atmos10120750

Growth rates obtained for waves from lidar measurements present 48.9% of negative values and 51.1% of positive values, showing a somewhat symmetric β distribution. We observe a maximal occurrence of waves in the range of $0< \beta <2$ (under saturated region) that represents 24% of the wave events observed in Na lidar profiles. Those waves presented amplification, but not as rapidly as $\sim \exp(\alpha z)$. It is also observed that ~35.6% of waves in lidar profiles are close of being saturated ($\beta \sim 0$).

For waves observed in imager data, we have found 61.5% of negative values and 38.5% of positive values, indicating larger amount of over-damped events. About 51.6% of these waves show strong attenuation ($\beta <$–6), while only ~9% of the waves observed in lidar dataset have similar growth rates. That difference may be caused by the method of analysis used by [8], which is biased towards waves that propagate normal to the wind flow, or are experiencing uniform Doppler shift along the Na layer. Also, ~15.4% of the waves are close to the saturation limit ($\beta \sim 0$), in contrast with waves observed in lidar data. Finally, the growth rate of imager-viewed AGWs show maximal occurrence in the interval of $-10< \beta <-8$ (over-damped region), which corresponds to 15.4% of the events.

4. Discussion

While freely propagating waves ($\beta >7$) correspond to 8.9% and 11.5% of the events observed in lidar and imager, respectively, about 90% of waves observed in both instruments show dissipative behavior (departures from the freely propagating wave growth rate α). The wave energy transferred to the media due to dissipative wave processes may cause several effects in the atmosphere, as mean flow acceleration and local heating. In general, hydrodynamic instabilities and diffusion processes are responsible to limit the wave amplitude.

The linear saturation theory (LST) predicts that the wave amplitude will reach the saturation limit when the horizontal perturbation velocity u' equals the intrinsic horizontal phase velocity of the wave c_i. The amplitude is then limited by convective or shear instabilities [13]. On the other hand, the diffusive filtering theory (DFT) states that waves will be severely damped by diffusion when the effective vertical diffusion velocity mD of the particles experiencing the wave motion exceeds the vertical phase velocity of the wave ωm^{-1} [14]. Here, D, m, and ω are the total effective atmospheric diffusivity, the vertical wavenumber and the wave frequency, respectively.

In this meaning, waves presenting $\omega > m^2 D$ propagate without attenuation, while waves presenting $\omega < m^2 D$ are removed from the spectra by diffusion. Our study as well as [8] suggest that gravity waves observed in lidar measurements are in accordance with DFT, while rules out the predictions of LST. However, some observed wave events in the lidar dataset presented peculiar behavior, suggesting that processes other than diffusivity have to be considered in order to explain the observed wave amplitude characteristics and growth rates.

5. Conclusion

Atmospheric gravity waves observed in lidar and imager measurements were analyzed in this study. An amount of 45 monochromatic waves were identified in lidar data, while 52 waves were obtained in images of mesospheric nightglow layers, respectively. The results showed that while each instrument samples a distinct region of the gravity wave spectra, about 90% of the events are of dissipative waves (for both datasets) .

Growth rate distributions are distinct for waves observed in different lidar to those observed in imager data. The maximal occurrence (24%) of lidar-observed waves is located in the under-saturated region where $0< \beta <2$, while the maximal occurrence of waves observed in the imager dataset (15.4%) is between $-10< \beta <-8$ within the over-damped region of the distribution.

Also, 51.6% of imager-observed waves were found in the strong dissipation region ($\beta <$–6), against only ~9% of these type of waves in the lidar dataset. Gravity waves observed in lidar density profiles support the diffusive filtering theory, which states the dissipation of wave energy is mainly due to diffusivity processes acting on the wave amplitude.

Author Contributions: Formal analysis, F.V.; Investigation, F.V. and G.Y.; Methodology, F.V. and G.Y.; Resources, G.Y., P.B. and D.G.; Writing – original draft, F.V.; Writing – review editing, F.V.

Funding: This research received no external funding by CNPq grant number 04/07695-5 and National Science Foundation under 1-NSF AGS Grant 17-59573 and 2-NSF AGS Grant 19-03336.

Acknowledgments: We are grateful to Capes, and FAPESP, the Brazilian Financial Agencies, that gave support to this work in several ways.

Conflicts of Interest: The authors declare no conflict of interest.

References

1. Fritts, D.C.; Alexander, M.J. Gravity wave dynamics and effects in the middle atmosphere. *Reviews of Geophysics* **2003**, *41*, [https://agupubs.onlinelibrary.wiley.com/doi/pdf/10.1029/2001RG000106]. doi:10.1029/2001RG000106.
2. Fritts, D.C.; Vadas, S.L.; Wan, K.; Werne, J.A. Mean and variable forcing of the middle atmosphere by gravity waves. *Journal of Atmospheric and Solar-Terrestrial Physics* **2006**, *68*, 247 – 265. Vertical Coupling in the Atmosphere/Ionosphere System, doi:https://doi.org/10.1016/j.jastp.2005.04.010.
3. Hines, C.O. Internal atmospheric gravity waves at ionospheric heights. *Canadian Journal of Physics* **1960**, *38*, 1441–1481. doi:10.1139/p60-150.
4. Swenson, G.; Liu, A.; Li, F.; Tang, J. High frequency atmospheric gravity wave damping in the mesosphere. *Advances in Space Research* **2003**, *32*, 785 – 793. Middle Atmosphere Structure and Dynamics, doi:https://doi.org/10.1016/S0273-1177(03)00399-5.
5. Taori, A.; Guharay, A.; Taylor, M.J. On the use of simultaneous measurements of OH and O_2 emissions to investigate wave growth and dissipation. *Annales Geophysicae* **2007**, *25*, 639–643. doi:10.5194/angeo-25-639-2007.
6. Reisin, E.R.; Scheer, J. Characteristics of atmospheric waves in the tidal period range derived from zenith observations of O2(0–1) Atmospheric and OH(6-2) airglow at lower midlatitudes. *Journal of Geophysical Research: Atmospheres* **1996**, *101*, 21223–21232, [https://agupubs.onlinelibrary.wiley.com/doi/pdf/10.1029/96JD01723]. doi:10.1029/96JD01723.
7. Clemesha, B.R.; Simonich, D.M.; Batista, P.P. A long-term trend in the height of the atmospheric sodium layer: Possible evidence for global change. *Geophysical Research Letters* **1992**, *19*, 457–460, [https://agupubs.onlinelibrary.wiley.com/doi/pdf/10.1029/92GL00123]. doi:10.1029/92GL00123.
8. Yang, G.; Clemesha, B.; Batista, P.; Simonich, D. Lidar study of the characteristics of gravity waves in the mesopause region at a southern low-latitude location. *Journal of Atmospheric and Solar-Terrestrial Physics* **2008**, *70*, 991 – 1011. doi:https://doi.org/10.1016/j.jastp.2008.01.013.
9. Medeiros, A.; Buriti, R.; Machado, E.; Takahashi, H.; Batista, P.; Gobbi, D.; Taylor, M. Comparison of gravity wave activity observed by airglow imaging at two different latitudes in Brazil. *Journal of Atmospheric and Solar-Terrestrial Physics* **2004**, *66*, 647 – 654. Dynamics and Chemistry of the MLT Region - PSMOS 2002 International Symposium, doi:https://doi.org/10.1016/j.jastp.2004.01.016.
10. Garcia, F.J.; Taylor, M.J.; Kelley, M.C. Two-dimensional spectral analysis of mesospheric airglow image data. *Appl. Opt.* **1997**, *36*, 7374–7385. doi:10.1364/AO.36.007374.
11. Gardner, C.S.; Voelz, D.G. Lidar studies of the nighttime sodium layer over Urbana, Illinois: 2. Gravity waves. *Journal of Geophysical Research: Space Physics* **1987**, *92*, 4673–4694, [https://agupubs.onlinelibrary.wiley.com/doi/pdf/10.1029/JA092iA05p04673]. doi:10.1029/JA092iA05p04673.
12. Vargas, F.; Swenson, G.; Liu, A.; Gobbi, D. O(1S), OH, and O2(b) airglow layer perturbations due to AGWs and their implied effects on the atmosphere. *Journal of Geophysical Research: Atmospheres* **2007**, *112*. doi:10.1029/2006JD007642.
13. Dewan, E.M.; Good, R.E. Saturation and the "universal" spectrum for vertical profiles of horizontal scalar winds in the atmosphere. *Journal of Geophysical Research: Atmospheres* **1986**, *91*, 2742–2748, [https://agupubs.onlinelibrary.wiley.com/doi/pdf/10.1029/JD091iD02p02742]. doi:10.1029/JD091iD02p02742.

14. Gardner, C.S. Diffusive filtering theory of gravity wave spectra in the atmosphere. *Journal of Geophysical Research: Atmospheres* **1994**, *99*, 20601–20622, [https://agupubs.onlinelibrary.wiley.com/doi/pdf/10.1029/94JD00819]. doi:10.1029/94JD00819.